NAVAL POSTGRADUATE SCHOOL

MONTEREY, CALIFORNIA

THESIS

CHARACTERIZATION OF HEAVY OXIDE INORGANIC SCINTILLATOR CRYSTALS FOR DIRECT DETECTION OF FAST NEUTRONS BASED ON INELASTIC SCATTERING

by

Philip R. Rusiecki

March 2015

Thesis Advisor: Craig F. Smith
Co-Advisor: Gamani Karunasiri

THIS PAGE INTENTIONALLY LEFT BLANK

REPORT DOCUMENTATION PAGE

Form Approved OMB No. 0704–0188

1. AGENCY USE ONLY *(Leave blank)*	2. REPORT DATE	3. REPORT TYPE AND DATES COVERED
	March 2015	Master's Thesis

4. TITLE AND SUBTITLE
CHARACTERIZATION OF HEAVY OXIDE INORGANIC SCINTILLATOR CRYSTALS FOR DIRECT DETECTION OF FAST NEUTRONS BASED ON INELASTIC SCATTERING

5. FUNDING NUMBERS

6. AUTHOR(S) Philip R. Rusiecki

7. PERFORMING ORGANIZATION NAME(S) AND ADDRESS(ES)
Naval Postgraduate School
Monterey, CA 93943-5000

8. PERFORMING ORGANIZATION REPORT NUMBER

9. SPONSORING /MONITORING AGENCY NAME(S) AND ADDRESS(ES)
N/A

10. SPONSORING/MONITORING AGENCY REPORT NUMBER

11. SUPPLEMENTARY NOTES The views expressed in this thesis are those of the author and do not reflect the official policy or position of the Department of Defense or the U.S. Government. IRB Protocol number ____N/A____.

12a. DISTRIBUTION / AVAILABILITY STATEMENT
Approved for public release; distribution is unlimited

12b. DISTRIBUTION CODE

13. ABSTRACT (maximum 200 words)

Heavy oxide inorganic scintillators may prove viable in the detection of fast neutrons based on the mechanism of inelastic neutron scattering. A candidate set of crystals incorporating constituents of heavy atomic mass, namely bismuth germinate (BGO), zinc tungstate (ZWO), cadmium tungstate (CWO), lead tungstate (PWO), lutetium-gadolinium orthosilicate activated with cerium (LGSO:Ce) and lutetium-aluminum garnet with cerium (LuAG:Ce), were characterized to reveal relevant properties for efficient fast neutron detection.

The optical measurements indicated strong transmittance with minimal absorption occurring in the visible spectrum. On average, the crystals achieved approximately 80% transmittance and 3% absorption, with the remaining light reflected at the air/crystal interface. Cathodoluminescence (CL) measurements with electron excitation energy of 5 keV provided information on the peak wavelength emission and light intensity. Results show that BGO and LGSO:Ce produced the highest scintillation light output and sharpest peak formation. Uncertain Ce^{3+} concentration and the presence of Eu^{3+} admixture caused LuAG:Ce to red shift and produce a false-positive bright emission. The gamma induced scintillation measurement yielded preliminary results showing stratification in light output based on incident energy in the range of 0.081–1.275 MeV. CWO and LGSO:Ce, crystals with similar structure, appeared less susceptible to this phenomenon.

14. SUBJECT TERMS
inelastic scattering, cathodoluminescence, heavy oxide inorganic scintillators, direct detection fast neutrons, gamma induced scintillation, scintillator crystals

15. NUMBER OF PAGES
61

16. PRICE CODE

17. SECURITY CLASSIFICATION OF REPORT	18. SECURITY CLASSIFICATION OF THIS PAGE	19. SECURITY CLASSIFICATION OF ABSTRACT	20. LIMITATION OF ABSTRACT
Unclassified	Unclassified	Unclassified	UU

NSN 7540–01-280-5500

Standard Form 298 (Rev. 2–89)
Prescribed by ANSI Std. 239–18

THIS PAGE INTENTIONALLY LEFT BLANK

Approved for public release; distribution is unlimited

CHARACTERIZATION OF HEAVY OXIDE INORGANIC SCINTILLATOR CRYSTALS FOR DIRECT DETECTION OF FAST NEUTRONS BASED ON INELASTIC SCATTERING

Philip R. Rusiecki
Major, United States Army
B.A., Franklin & Marshall College, 1997

Submitted in partial fulfillment of the
requirements for the degree of

MASTER OF SCIENCE IN APPLIED PHYSICS

from the

NAVAL POSTGRADUATE SCHOOL
March 2015

Author: Philip R. Rusiecki

Approved by: Craig F. Smith
Thesis Advisor

Gamani Karunasiri
Thesis Co-Advisor

Andres Larraza
Chair, Department of Physics

THIS PAGE INTENTIONALLY LEFT BLANK

ABSTRACT

Heavy oxide inorganic scintillators may prove viable in the detection of fast neutrons based on the mechanism of inelastic neutron scattering. A candidate set of crystals incorporating constituents of heavy atomic mass, namely bismuth germinate (BGO), zinc tungstate (ZWO), cadmium tungstate (CWO), lead tungstate (PWO), lutetium-gadolinium orthosilicate activated with cerium (LGSO:Ce) and lutetium-aluminum garnet with cerium (LuAG:Ce), were characterized to reveal relevant properties for efficient fast neutron detection.

The optical measurements indicated strong transmittance with minimal absorption occurring in the visible spectrum. On average, the crystals achieved approximately 80% transmittance and 3% absorption, with the remaining light reflected at the air/crystal interface. Cathodoluminescence (CL) measurements with electron excitation energy of 5 keV provided information on the peak wavelength emission and light intensity. Results show that BGO and LGSO:Ce produced the highest scintillation light output and sharpest peak formation. Uncertain Ce^{3+} concentration and the presence of Eu^{3+} admixture caused LuAG:Ce to red shift and produce a false-positive bright emission. The gamma induced scintillation measurement yielded preliminary results showing stratification in light output based on incident energy in the range of 0.081–1.275 MeV. CWO and LGSO:Ce, crystals with similar structure, appeared less susceptible to this phenomenon.

THIS PAGE INTENTIONALLY LEFT BLANK

TABLE OF CONTENTS

THIS PAGE INTENTIONALLY LEFT BLANK

LIST OF FIGURES

LIST OF TABLES

THIS PAGE INTENTIONALLY LEFT BLANK

LIST OF ACRONYMS AND ABBREVIATIONS

A	atomic mass number
Ba	barium
Bi	bismuth
BGO	bismuth Germinate ($Bi_4Ge_3O_{12}$)
CWO	cadmium tungstate ($CdWO_4$)
Ce	cerium
Cf	californium
CL	cathodoluminescence
Co	cobalt
E_g	bandgap energy
E_{ph}	photon energy
e-h	electron-hole
eV	electron volt
GaAsP	gallium arsenide phosphide
IND	improvised nuclear device
keV	kilo-electron volt (10^3)
LGSO	lutetium gadolinium orthosilicate ($Lu_2Gd_2SiO_5$)
LuAG	lutetium aluminum garnet ($Lu_3Al_5O_{12}$)
MeV	mega-electron volt (10^6)
PWO	lead tungstate ($PbWO_4$)
PMT	photomultiplier tube
Pu	plutonium
SEM	scanning electron microscope
WMD	weapons of mass destruction
Z	atomic number
ZWO	zinc tungstate ($ZnWO_4$)

THIS PAGE INTENTIONALLY LEFT BLANK

ACKNOWLEDGMENTS

The education I received at the Naval Postgraduate School gave me a tremendous opportunity to learn, mature and expand my critical thinking skills in what were unfamiliar and often uncomfortable subject areas. Without the support and encouragement of NPS professors, administrators, staff and fellow students, my success would not be possible. Professor Richard Harkins, Dr. Nancy Haegel, Dr. Peter Crooker, Dr. Joseph Hooper, Dr. James Luscombe and Dr. Brett Borden are standout educators who happily entertained my questions and provided a level of feedback that greatly contributed to the completion of this thesis.

Dr. Gamani Karunasiri, my thesis co-advisor, fielded a daily assault of questions, yet returned insightful explanations, answers, and much-needed reassurance. Thank you for always making time to listen to my concerns. I am also grateful to Dr. Fabio Alves and Mr. Carl Oros for making their equipment and laboratories available for my use.

The incredible guidance I received from my thesis advisor, Dr. Craig Smith, is a result of his passion for educating military officers in science-related areas of national security. His extensive background and experience in the nuclear physics community is humbling, and it was an honor to learn from his firsthand knowledge and practical skill. Thank you for allowing me to work on your team.

My mother and father inspired me to always do my best and not be afraid of trying; I believe this accomplishment fulfills that challenge.

I am forever grateful to my wife, Emily, for her patience, understanding and encouragement during these graduate school years. Without her love and commitment, I would not have obtained this goal. As for my son, Corbin, I did this for you. The importance of education—setting difficult goals and working tirelessly to achieve them—is what I hope you learn from my endeavors. The world is whatever you make of it, and nothing worthwhile comes easily.

THIS PAGE INTENTIONALLY LEFT BLANK

I. INTRODUCTION

A. MILITARY RELEVANCE

Preventing nuclear terrorism is a key objective for both national and international security. According to the 2010 United States National Security Strategy, weapons of mass destruction (WMDs) (particularly nuclear weapons) continue to pose "the gravest danger to the American people and global security," with explicit emphasis placed on the need to prevent terrorists from acquiring, smuggling and ultimately, employing weapons-grade material in an improvised nuclear device (IND) [1]. Even though nuclear weapons were developed by way of enormous nation-sponsored programs such as the Manhattan Project, the current terrorist threat relies on both stolen or illegally procured technology and materials [2]. Significant improvement in the ability to detect special nuclear material will greatly assist the ongoing effort to prevent a catastrophic event involving a rogue nuclear device.

This research is intended to provide the military community, specifically ongoing research at the Naval Postgraduate School, with valuable insights related to fast neutron detection. The ultimate goal of developing sensors able to directly measure sources of fissile material has immediate applications from a homeland security perspective, specifically port and border security and sea interdiction operations, as well as for worldwide WMD elimination missions. Combatting WMDs remains a national priority, and improvements in detection technology will contribute to that endeavor.

B. PURPOSE OF THESIS

Detecting fast neutrons through the process of inelastic scattering in heavy oxide inorganic scintillators has the potential to significantly increase neutron detection efficiency and is the central theme of this thesis. Scintillators containing heavy atomic constituents such as bismuth, lead, tungsten and lutetium perform two key functions not generally encountered with other types of neutron detection technology. First, they increase the inelastic scattering cross section for fast neutrons, resulting in gamma photon emission(s) via the (n, n'γ) reaction. This process provides a signal from the neutron

interaction without the typical intermediate step of thermalization, and is therefore a more direct method of detection than those that rely on both thermalization and absorption. Second, the resulting gamma photons and associated ionization processes trigger scintillation within the same crystal, enabling data analysis to determine the neutron flux [3]. This efficient detection method is well suited for applications involving incident neutrons of high energy, such as those resulting from spontaneous fission of certain isotopes of plutonium and uranium.

Through an ongoing, informal collaboration with the Institute for Scintillation Materials at the National Academy of Sciences of Ukraine, a candidate set of scintillator crystals was obtained. In this research, these candidate crystals were subjected to initial characterization testing using cathodoluminescence and photo-absorption measurements. Preliminary measurements of their scintillation response to various laboratory radiation sources were also carried out. The approach and results of these measurements are discussed in greater detail throughout this work. Table 1 provides some pertinent summary data pertaining to the studied scintillator crystals.

Table 1. Candidate set of scintillator crystals obtained from the Institute for Scintillation Materials, Ukraine, from [4].

Scintillator based on	Chemical Formula	Abbreviation	Dimensions (mm)	Activated
Bismuth Germanate	$Bi_4Ge_3O_{12}$	BWO	20x30x11	No
Lead Tungstate	$PbWO_4$	PWO	22x22x10	No
Cadmium Tungstate	$CdWO_4$	CWO	20x20x20	No
Zinc Tungstate	$ZnWO_4$	ZWO	20x20x20	No
Lutetium-Gadolinium Orthosilicate	$Lu_2Gd_2SiO_5(Ce)$	LGSO:Ce	20(dia) x 10	Yes, 0.3% Cerium
Lutetium-Aluminum Garnet	$Lu_3Al_5O_{12}(Ce)$	LuAG:Ce	20(dia) x 10	Yes, 0.001% Cerium

C. RESEARCH OBJECTIVES AND GOALS

The broad objective of this research is to examine a candidate set of heavy oxide inorganic crystal scintillators to better understand the potential use of inelastic scattering to detect fast neutrons. This method of fast neutron detection holds significant promise when applied to sources of combined gamma and neutron radiation—a situation encountered with fissile materials and other spontaneous fission isotopes such as Cf-252 and Pu-240. The crystals not only provide the site upon which gamma photons produce scintillation, but they also enhance the process of inelastic scattering of incident fast neutrons within the same crystal, resulting in the emission of additional gamma photons that likewise cause scintillation [4]. The specific goals of this research are to:

- explore the physics of fast neutron inelastic scattering for the candidate set of scintillators;
- examine the process of scintillation for incident and generated gamma photons and investigate the results of preliminary experimentation;
- compare results of cathodoluminescence and photo-absorption measurements of the candidate crystals and compare the results to those of previous works; and
- observe and quantify the scintillation response of the candidate crystals to stimulation by available radiation sources.

THIS PAGE INTENTIONALLY LEFT BLANK

II. BACKGROUND THEORY

A. NEUTRON INTERACTIONS

Fundamentally, neutrons are detected through their reactions based on absorption, scattering or other interactions, with the key discriminator being the energy of the incident neutrons as they enter the detection medium [5, pp. 537–538]. Neutrons generally reside in the nucleus of atoms and carry no electrical charge, but they can be liberated through a variety of reactions, including the interaction between alpha radiation and materials such a beryllium (α, n); photoneutron (γ, n) stimulation; fission (spontaneous or induced); and fusion processes, among others. Once freed, neutrons are unstable against β decay and have a half-life of 10.6 minutes. By convention, neutrons are grouped into four categories based on their energy [6], as shown in Table 2.

Table 2. Classification of neutrons by energy, from [6].

Nomenclature	Energy
Thermal	≈ 0.025 eV
Epithermal	~ 1 eV
Slow	~ 1 keV
Fast	= 100 keV–10 MeV

An extremely important aspect regarding free neutrons lies in the understanding that most liberating reactions produce a broad spectrum of neutron energies rather than discrete, mono-energetic values [7]. This is true in particular for the spontaneous fission reactions of transuranic isotopes such as Cf-252, as shown in Figure 1 [8]. This phenomenon inherently makes detecting neutrons of various incident energies a challenge with existing detection technologies that are based on either absorption of thermal neutrons, scattering of fast neutrons or a combination of the two. Detection efficiency and sensitivity are therefore two important characteristics of detector systems.

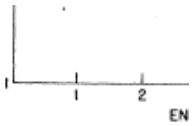

Figure 1. Experimentally determined energy spectrum of Cf-252 fission neutrons, from [8].

1. Absorption Reactions

Absorption, also known as neutron capture, is an indirect process of great significance for neutron detection,[1] and generally occurs at thermal or near thermal energy levels. Several types of reactions exist to convert incident neutrons into easily quantifiable products, including charged particles and gamma radiation, and include the $^{10}B(n, \alpha)$, $^{6}Li(n, \alpha)$, $^{3}He(n, p)$ reactions, as well as neutron capture (n, γ), neutron-induced fission and others [5, pp. 505–535]. The BF_3 tube, for example, detects thermalized neutrons from the $^{10}B(n, \alpha)$ reaction. These methods require the incident neutrons to react with the given target (B, Li, He, Cd, Gd, etc.) and produce charged particles or gamma radiation products that are then detected and analyzed. As mentioned, neutron absorption is most appropriate for thermal neutrons; in the case of more energetic neutrons, detection

[1] Indirect in the sense that the interaction medium (such as cadmium or gadolinium) may be different than the medium in which the resulting gamma radiation or other reaction products are registered; also in the sense that, in the case of fast neutrons, moderation is normally required before the absorption event can take place with high cross section.

based on absorption generally requires that the neutrons be "thermalized" prior to absorption. In such cases, this results in reduced detection efficiency since the process of thermalizing the more energetic neutrons provides opportunities for them to evade detection by escape from the detection medium [9]. Figure 2 illustrates how the probability, or cross section, of the reactions for ^{10}B, ^{6}Li and ^{3}He are dramatically reduced with increased neutron energy. This is primarily due to the 1/v (i.e., the reciprocal of the neutron velocity) dependence on these reaction cross sections over much of the energy range [5, p. 507].

Figure 2. Cross section as a function of neutron energy (eV) for the $^{10}B(n, \alpha)$, $^{6}Li(n, \alpha)$ and $^{3}He(n, p)$ reactions, from [5, p. 508].

2. Elastic Scattering

When neutron energies exceed the realistic cross section for absorption, generally in the low keV range, a different conversion process, elastic scattering, becomes predominant. Target nuclei with low atomic mass numbers (A) provide the best media for elastic scattering, with hydrogen being the most preferred [5, p. 537]. Also according to [5], the process occurs when an incident neutron with appreciable kinetic energy transfers a portion of its energy to the target nucleus, causing it to recoil. The resulting recoil nucleus, [5] reports, is essentially a charged particle able to ionize surrounding material, and the incident neutron scatters to a lower energy. This process continues until the

neutron is either reduced to the thermal threshold (i.e., where the cross section becomes attractive for absorption reactions), or the neutron escapes the material (neutron loss). Applying the laws of conservation of energy and linear momentum, the ratio between final and initial neutron energy in an elastic scattering event is given by [6]:

$$\frac{E'}{E} = \frac{A^2 + 1 + 2A\cos\theta}{(A+1)^2} \tag{1}$$

where E′ is the final neutron energy, E is the initial neutron energy, A is atomic mass of the target nucleus and θ is the scattered angle. When no scattering deflection occurs, (θ = 0), E′ / E = 1 and no energy is exchanged. The maximum energy exchange occurs at θ = 180° and the equation simplifies to [5, pp. 553–554]:

$$E'_{\max} = \left(\frac{A-1}{A+1}\right)^2 E \tag{2}$$

For hydrogen (A = 1), all of the neutron energy is transferred in a single head-on collision, while heavier atoms such as uranium (A = 238) realize a minimal energy exchange (~ 0.0167E) that would require numerous elastic collisions in order for a fast neutron to become fully thermalized.

Elastic scattering of fast neutrons can therefore serve two purposes: set the conditions for absorption reactions by thermalization, or act as a standalone detection method. However, the intrinsic efficiency of fast neutron detectors using elastic scattering via a single CH_4 or ^4He tube is approximately 1%, and the reaction cross sections are about two orders of magnitude lower than those of detection using neutron absorption reactions [10]. Furthermore, thermalizing fast neutrons for absorption reactions prevents a rapid detection signal due to the multiple collisions that must occur within the moderator, and also adds size and weight to the detector [4], [5].

3. Inelastic Scattering

The efficient detection of fast neutrons, therefore, requires a different approach than capitalizing on neutron absorption and elastic scattering. The phenomenon of inelastic scattering offers such an approach. At threshold neutron energies (E_{th}) close to or above ~ 1 MeV, the cross section for inelastic scattering of fast neutrons becomes

appreciable. Below this threshold, E_{th} < ~ 1 MeV, only elastic scattering can occur. Inelastic scattering is the process by which an incident neutron is briefly absorbed by the target nucleus but then quickly re-emitted, leaving a residual energy of excitation that the nucleus then sheds in the form of one or more photon emissions [11]. At energies greater than E_{th}, the cross section for inelastic scattering constitutes approximately one third to one half of the total cross section for all scattering events and increases with the atomic number (Z) of the target nuclei as Figure 3 illustrates. The cross section increases with Z number because of both the increased geometrical size of the nuclei, and the larger number of possible excitation levels [12].

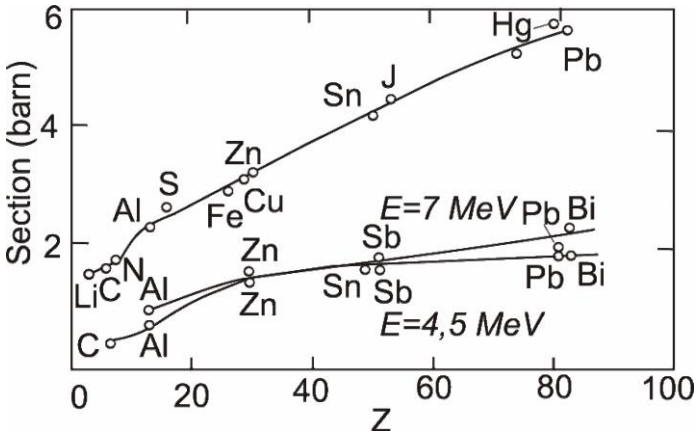

Figure 3. Inelastic scattering cross section (lower curves) of target nuclei with atomic number (Z) for the neutron energies 4.5 MeV and 7 MeV. Total interaction cross section values are given by the upper curve, from [12].

Figure 3 demonstrates the Z dependence on scattering cross section at two discrete neutron energy values, E_n = 4.5 MeV and 7 MeV. It is interesting to note that a 55% increase in neutron energy only weakly increases the inelastic cross section; the more significant dependence clearly lies with the increased Z number. Consequently, for incident neutron energies that exceed E_{th}, an increased likelihood of inelastic scattering interactions can be expected in scintillators with heavy atomic constituents.

Scintillation triggered by fast neutron inelastic scattering will therefore produce a rapid response without the inefficiencies associated with the requirement for

thermalization. It has been shown that inelastic scattering of fast neutrons incident upon heavy nuclei can transfer a substantial percentage of energy with minimal collisions as Figure 4 demonstrates [12]. The (n, n'γ) reaction (i.e., inelastic scattering), produces γ (gamma) photons and scattered secondary neutrons of substantially lower energy. In the example shown in Figure 4, it can be seen that an initial neutron distribution centered on ~14 MeV produces a transformed distribution with a peak near 1–2 MeV following interaction with Bi. With additional inelastic and elastic scattering, scattered neutrons with $E_n << 1$ MeV can react in the (n, γ) radiative capture reaction and generate additional scintillations [6]. Previous studies have shown the detection efficiency of the γ photons reaches 70–80%, with neutron detection efficiency not less than 40% for crystals similar to the candidate set of scintillators in this research [3].

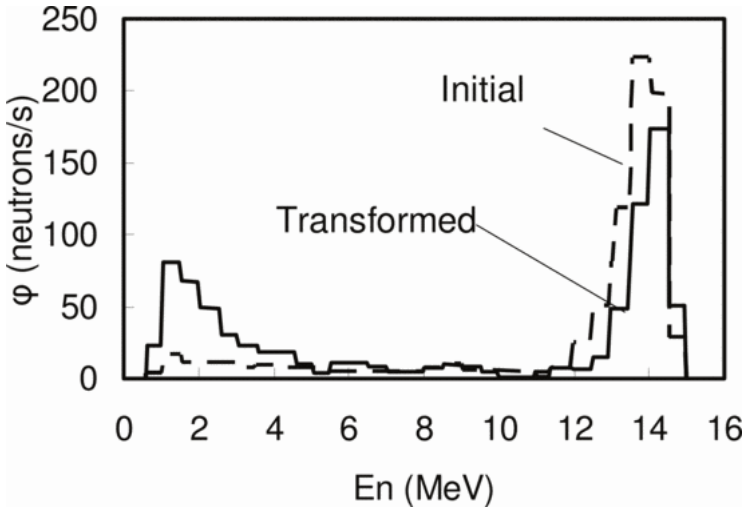

Figure 4. Transformation of the neutron spectrum for inelastic scattering on Bi (solid line). The dashed line is the spectrum prior to scattering event, from [12].

B. SCINTILLATION

Generating γ photons through the process of fast neutron inelastic scattering is the first step leading to scintillation. The processes described in the previous section occur on a timescale measured in nanoseconds, due to the efficient and direct manner in which fast neutrons interact with the heavy atomic constituents within the crystal [5, pp. 545–546]. For the purposes of this thesis, the scintillation process is considered one in which

ionizing radiation excites a scintillating material which has the special characteristic of relaxing from that excited state by releasing/emitting light. The scintillators in this study are classified as insulators due to their bandgap energy of > 5 eV. Some terminology usually associated with solid state semiconductor physics is applicable to the discussion of the ionization process; however, it is not intended to imply that heavy oxide inorganic scintillators are semiconductors.

1. The Ionization Process

Assuming that the scintillator is initially in a state of near equilibrium at the time of the inelastic scattering event (i.e., (n, n' γ) reaction), the emitted γ photons will interact with atoms in the crystalline structure of the scintillator to produce free or quasi-free electrons [13, p. 2], as Figure 5 illustrates. The energy of the primary ejected electron is equal to the difference between the γ photon energy and the binding energy of the electron in its orbital.

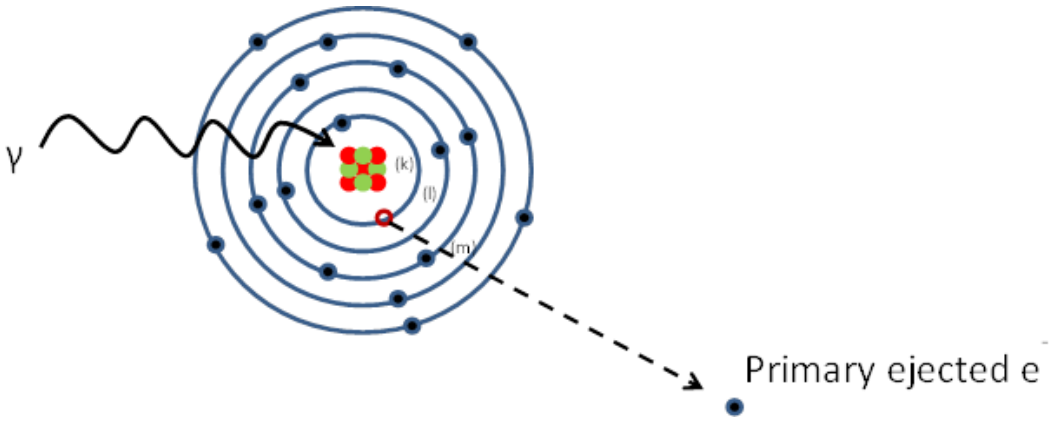

Figure 5. Incident γ photon, with $E_\gamma = h\nu$, incident upon an atom in the crystalline structure. Ejected primary electron energy is $E_e = (h\nu - E_{binding})$.

The ionized atom can relax either radiatively by emitting a photon, as Figure 6 demonstrates, or non-radiatively by generating secondary electrons through the Auger effect. The latter process has a greater probability [13, p. 3], and is shown in Figure 7. The resulting secondary photons from the radiative relaxation have energies in the x-ray portion of the spectrum and can cause further ionization events in other atoms within the

lattice [13, p. 4]. Their energy is equal to the difference between the binding energies of the upper and lower electron orbitals.

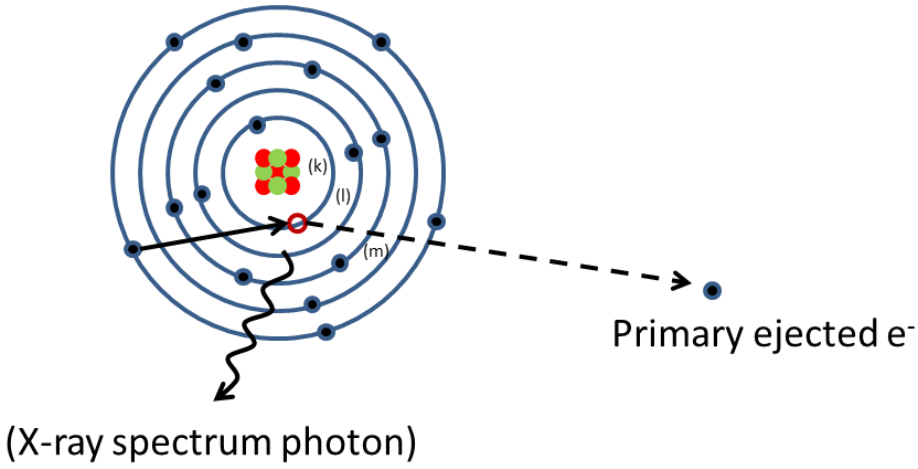

Figure 6. Atom with ionized inner shell relaxed radiatively by emitting a secondary photon in the x-ray portion of the spectrum.
$E_{xray} = E_{upper} - E_{lower}$.

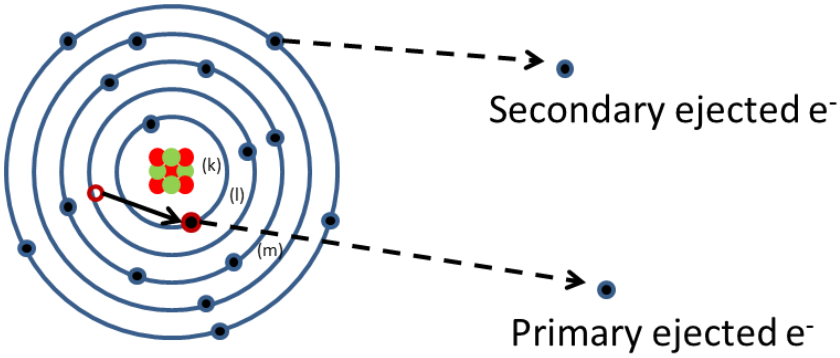

Figure 7. Atom with ionized inner shell relaxed non-radiatively by generating secondary electrons (Auger effect), and holes in the valence band. The energy of the secondary electrons is
$E_{sec} = (E_{upper} - E_{lower}) - E_{binding\ Auger}$.

2. Luminescence

The net result of these processes is an avalanche of electron (holes) and photon emissions that continue until further ionization is not possible (i.e., electron energy falls below the crystal's ionization threshold). Electrons migrate to the bottom of the

conduction band and holes move to the top of the valence band where electron-hole (e-h) pair energy ultimately equals the bandgap energy (E_g) for the crystal [13, pp. 4–5]. Luminescent centers, whether intrinsic or extrinsic, provide the location for the radiative transition from an excited state to a lower (ground) state through the release of photons in the visible or near visible spectrum [14]. Intrinsic luminescent centers are native to the material, involve band-to-band recombination of e-h pairs, and are attributed to lattice defects or anion vacancies within the crystal [14]. Extrinsic luminescence exists when rare earth ions and/or transition metals are deliberately added to the material for the purpose of creating luminescent centers [15]. For the candidate set of scintillators in this study, CWO, PWO and ZWO (compounds with the complex anion WO_4^{2-}) exhibit intrinsic luminescence, while the activated crystals of LuAG:Ce and LGSO:Ce are extrinsic due to the addition of the Ce^{3+} ions. BGO is considered self-activating, and displays properties of both intrinsic and extrinsic luminescence [13, pp. 8–9].

3. The Role of Activators

The extrinsic luminescent scintillators included in this study contain Ce^{3+} ions, which are referred to as activators, and the energy band structures of these materials are graphically displayed in Figure 8. They are responsible for transition sites in what is normally the bandgap region of the crystal [5, pp. 231–232]. Without an activator, transitions can only occur across the entire bandgap, a process that is inefficient due to the physical separation of electrons and holes within the conduction and valence bands. In the pure crystal, there is no physical means by which to fix electrons in order to efficiently permit recombination; probability dictates the likelihood of e-h pair generation [16]. The activator provides at least one capture site that serves to fix an electron and increase e-h pair recombination [16]. Since the photon energy $E_{ph} < E_g$, and the typical bandgap for the set of scintillators in this study is ~ 5 eV, it is more likely that the emitted photons will fall within the visible or near visible spectrum.[2] Although scintillation response (i.e., optical emission) in inorganic scintillators is an intrinsic property unique to

[2] Since E = 1240 nm / λ, then at the bandgap of 5 eV, λ = 248 nm. However, if $E_{ph} < E_g$, then the potential exists for E_{ph} to be within the visible spectrum (e. g., E_{ph} = 2.5 and λ = 498 nm).

each crystalline compound, it is expected that activated scintillators will display higher levels of visible light output than non-activated ones.[3]

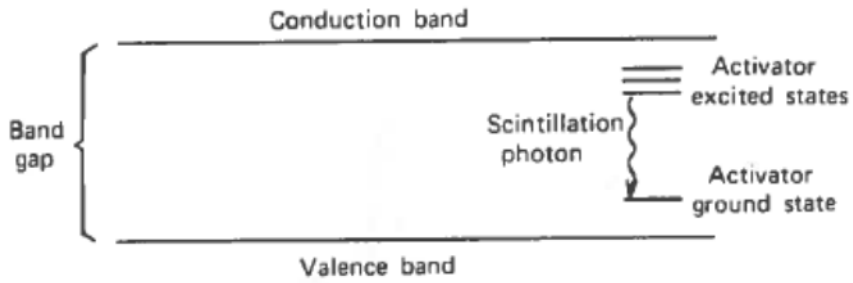

Figure 8. Energy band structure of an activated crystalline scintillator, from [5, p. 232].

In summary, scintillation itself involves a complex series of events best summarized at the macroscopic level by the following passage:

> As a general idea of the scintillation process, consider it as the conversion of the energy of an incident gamma-quantum or particle into a great many low energy photons. After an ionization event a scintillator is in a non-equilibrium state and begins to relax toward a new equilibrium. Such a relaxation occurs by a multitude of elementary processes such as a creation of primary electronic excitation which will produce an avalanche of secondary excitations including electrons, holes, photons, and plasmons. These electronic excitations produce numerous thermalized electron-hole (e-h) pairs and low energy excitons which ultimately transform into light photons, i.e., scintillation. [13, p. 1]

A thorough discussion of the scintillation process, to include e-h pair creation, excitation and emission of luminescent centers is available in [13] and [14].

[3] This assumption is valid only when comparing crystals of the same basic chemical makeup, with the difference being the addition of an activator ion. The activator must be chosen with care to ensure that the resulting activator sites will produce photons in the visible range. Activators alone do not ensure added efficiency or increased visible light output.

III. EXPERIMENTAL RESULTS

A. OPTICAL CHARACTERIZATION

One important consideration in the characterization of inorganic scintillators involves the optical properties of the material, notably the index of refraction *n* and the rate of transmission [13, p. 31]. In order for a photon to reach the intended detector, it must traverse the crystal with minimal absorption, reflection or scattering. For the candidate set of crystals in this study, *n* is relatively high[4] and ranges from 1.8–2.3. Therefore, it is expected that some light is lost to reflection at the air/crystal interface since *n* for air is ~ 1. Since this experiment seeks to ascertain the rate of transmission and percentage of photo absorption, correcting for changing *n* values is not necessary, but is certainly a consideration in detector design [13, p. 32].

1. Laboratory Setup

The laboratory setup used to measure the rate of transmission is shown in Figure 9. Light incident from a 250 W quartz halogen light source traverses the scintillator crystal where the spectrometer then records and sends the data to the Spectra Suite™ software program for analysis [17]. Measurement of light transmitted and reflected were recorded and used to determine the percentage of light absorbed within the crystal. Photon intensity equals the sum of photon transmission, reflection and absorption, as the following equation indicates [18]

$$I_o = I_t + I_r + I_a \tag{3}$$

where I_o is the initial photon intensity, and I_t, I_r and I_a equal photon intensity transmitted, reflected and absorbed, respectively.

[4] The index of refraction for the candidate set of crystals is high when compared to glass (n ~ 1.5), but is within the same general range as other solid inorganic scintillator crystals.

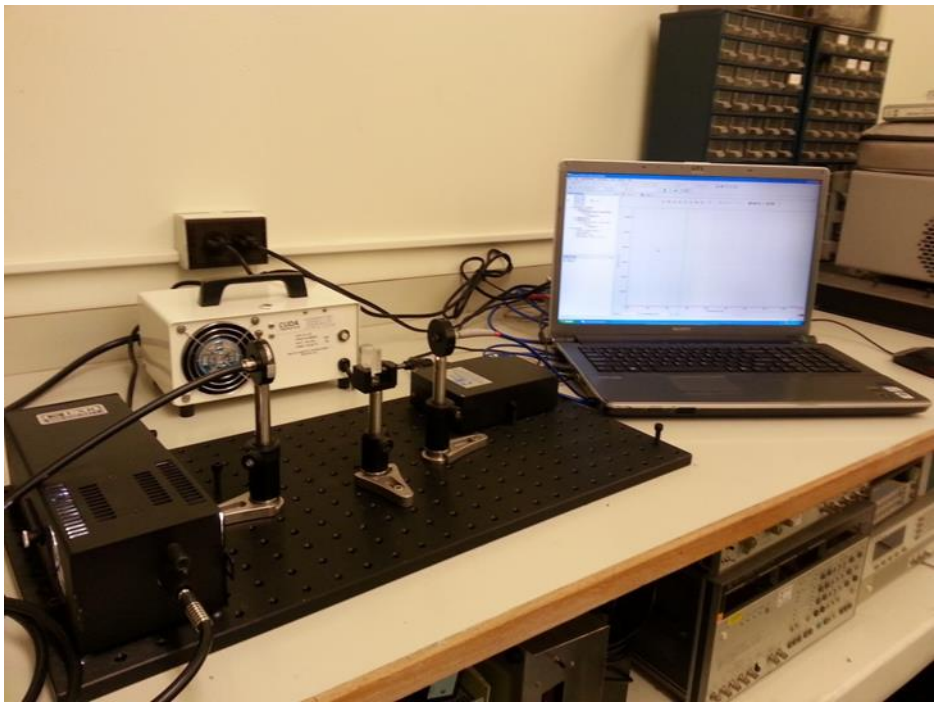

Figure 9. Ocean Optics, Inc. HR2000+CG–UV–NIR high resolution spectrometer laboratory setup.

A high rate of transmission is desirable in scintillators for two purposes. First, it ensures that emitted photons from the inelastic neutron scattering will not be absorbed or unintentionally reflected in the crystal. It also permits scintillated photons, now in the visible or near visible spectrum, to reach the intended photodetector device. Photon loss in either step reduces efficiency [13, p. 31].

Transmittance T is the fraction of incident light that passes through the crystal and is simply the ratio of transmitted to initial light intensity [18].

$$T = \frac{I_t}{I_o} \tag{4}$$

2. Results

The results of the transmission measurements are shown in Figure 10. All crystals display a strong transmittance that exceeds 0.70, with LGSO:Ce, CWO and LuAG:Ce achieving 0.85 or greater.

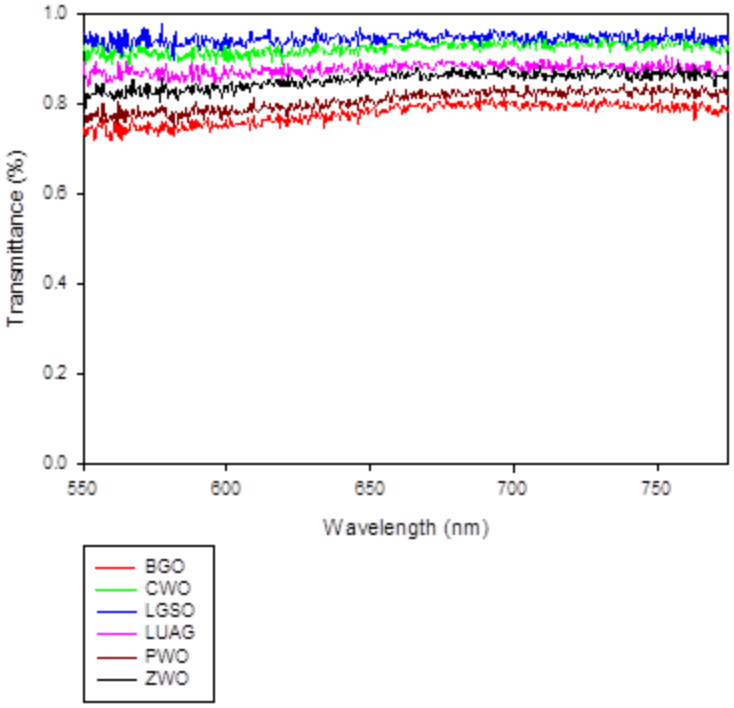

Figure 10. Transmittance *T* for the candidate set of scintillators. All crystals exceed 70% light transmittance, with several achieving 85% or higher.

For comparison, Figure 11 is provided from [19] to show the strong agreement in *T* for a representative collection of inorganic scintillators that includes BGO and PWO from this study. It is interesting to note that the solid black dots represent the theoretical limits of *T* based on multiple bouncing between two parallel end surfaces and no internal absorption [19]. The calculations used in [19] are

$$T_s(\lambda) = \frac{1 - R(\lambda)}{1 + R(\lambda)} \tag{5}$$

where reflectance R is

$$R(\lambda) = \frac{[n(\lambda)_{crystal} - n(\lambda)_{air}]^2}{[n(\lambda)_{crystal} + n(\lambda)_{air}]^2} \tag{6}$$

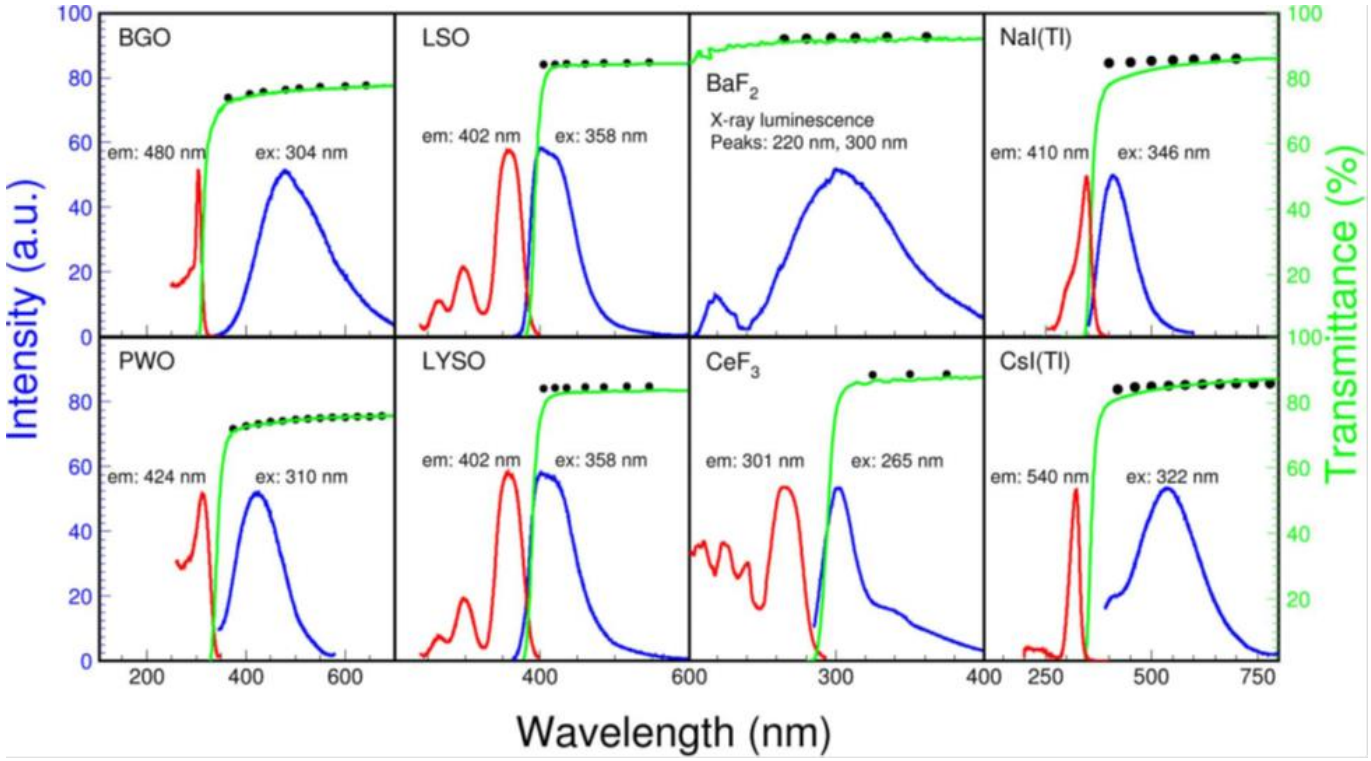

Figure 11. Excitation (red), photo-luminescence (blue) and optical transmittance (green) are shown as a function of wavelength for heavy crystal scintillators. The solid black dots represent the theoretical limit of the transmittance, from [19].

It can be seen from Figure 11 that the difference between the theoretical and experimental *T* is small, and attributed to internal absorption. To further support this claim, Figure 12 shows the percentage of absorption measured in BGO from this study. A simple rearranging of terms from [18] yields the equation for photon absorption.

$$I_a = I_o - I_t - I_r \tag{7}$$

The absorption of light in BGO is representative of all the candidate crystals in this study, with peak absorption not exceeding ~ 5% and mostly averaging ~ 2–3%. This finding is in strong agreement with the results measured in [19].

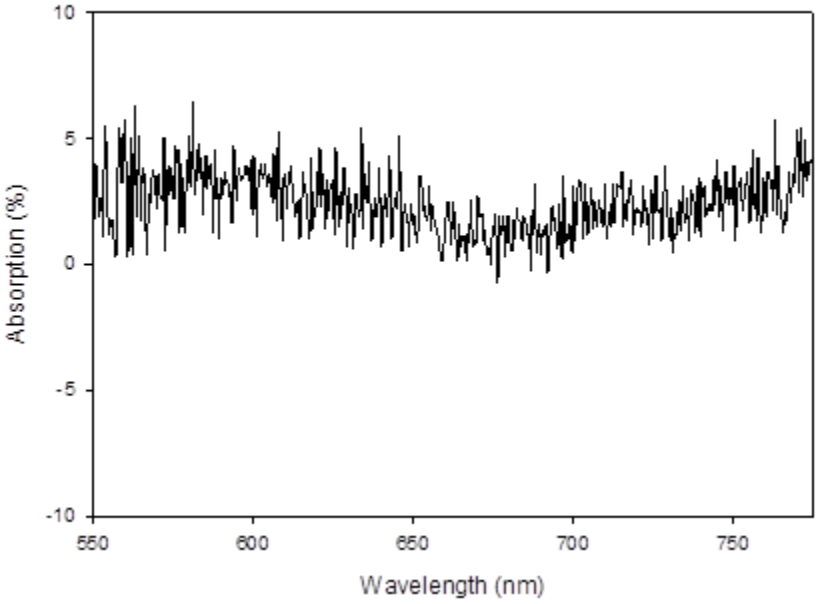

Figure 12. Photon absorption as a function of wavelength for BGO in the visible and near visible spectrum.

Based on measurements recorded in this experiment, the set of scintillator crystals in this study achieved high transmittance and low absorption of visible and near visible light. On average, 80% of light traversed the crystals and less than 3% was absorbed. The remaining light loss is attributed to reflection at the air/crystal interface and is due to the relatively high index of refraction for the scintillator crystals. The findings in this

experiment are in strong agreement with the cited works when comparing overlapping scintillators.

B. CATHODOLUMINESCENCE CHARACTERIZATION

In the simplest terms, cathodoluminescence (CL) is the emission of photons from a material under excitation by an electron beam [2]. The photons are emitted at characteristic wavelengths from the material when it is subjected to electron bombardment. The CL measurements were conducted with the use of a scanning electron microscope (SEM) [20]. The theory of CL is similar to that described in Chapter II involving the scintillation process insofar as the bombarding electrons (vice gamma photons) facilitate a transfer of energy to electrons in the crystalline lattice resulting in the production of valence holes and conduction band electrons [20]. The resulting e-h pair generation, recombination and photon emission process in CL is otherwise similar to scintillation.

There are several quantitative benefits associated with CL measurements for the characterization of heavy inorganic scintillators. CL provides a spectral response spanning the desired wavelength domain, which is used to identify peak photon emission wavelengths [21]. According to [14, p. 43], scintillators with photon emission in the visible or near visible spectrum are preferred for detection by a photocathode (PMT); therefore, the wavelength domain for this study ranged from approximately 350–750 nm. In addition to peak photon emission, CL also measures the intensity, or photon count, at a given wavelength. Intensity of photon emission is among the most important factors in the scintillation process [14]; a weak response signal indicates poor scintillation yield based on the relative light output defined as

$$L_R = \frac{N_{ph}}{E_{inc}} \tag{8}$$

where L_R is the number of photons emitted by the scintillator per unit of absorbed energy (usually 1 MeV), N_{ph} is the number of emitted photons and E_{inc} is the energy attributed to the radiation source [13, p. 20].

From the perspective of quality control, CL can also aid in the identification of contaminates, known as admixtures, that are inadvertently incorporated during the crystal growth process. Admixtures can undermine the performance of scintillators through false positive readings, and are discussed in the results for LuAG:Ce. When used as a quality control and quality assurance parameter, CL is a valuable test to ensure that a homogeneous crystalline matrix exists.

1. Laboratory Setup

The laboratory setup used for the CL measurements is shown in Figure 13. The SEM is a JEOL model 840A and is operated in the spot mode, meaning the electron beam is held in a static position and incident normal to the sample. The excitation energy varied between 5–20 keV; however, lower energy proved optimal due to unwanted electrical charging encountered at higher energies. A probe current of 6×10^{-11} A and magnification from 600× to 1300× was used. An Oxford CL system with a 0.25 m path length monochromator performed the spectroscopy. The detector is a thermoelectrically cooled photomultiplier with a response range from 300–900 nm.

Figure 13. JEOL 840A SEM with Oxford CL system laboratory setup.

2. Results

The experimentally derived peak wavelength emissions are in reasonable agreement with Lecoq's values given in [14, pp. 23–26], and are provided in Table 3. All of the candidate crystals displayed peak photon emission in the visible spectrum, but due to discrepancies in crystal growth techniques, some variations in the accepted values exist in the literature. Furthermore, for the Ce activated crystals, [14] provides no information concerning Ce concentrations, an important consideration discussed in the following paragraphs.

Table 3. Experimentally determined peak wavelengths for the candidate set of crystals using CL at 300 K.

Scintillator	λ_{max} (nm) – Lecoq [14]	λ_{max} (nm) – Experimental
BGO	505	518
PWO	420	433
CWO	495	475
ZWO	480	504
LGSO:Ce	420-430	416
LuAG:Ce	520	630

Although most of the candidate crystals display peak emission wavelengths close to the accepted values given in Table 3, LuAG:Ce clearly exhibits a red shift from the literature [21], as Figure 14 illustrates. According to [21], peak photon emission is achieved at 545 nm with a 0.03% Ce concentration. However, in [22], H. Li et al. suggest that varying Ce concentrations may contribute to wavelength shifts. In [22], the maximum intensity and peak wavelength (545 nm) are measured at a Ce concentration of 0.5%, with red shift occurring as Ce concentrations decrease. Applying this rational, LuAG:Ce in Figure 14 should be red shifted to some wavelength greater than 545 nm since the Ce concentration is only 0.03%. Figure 15 depicts this red shift for varying Ce concentrations of LuAG:Ce using X-ray radioluminescence, with Ce concentrations greater than 0.5% resulting in quenching [22]. To further support this claim, Dr. Oleg

Sidletskiy[5] stated that the LuAG:Ce sample used in the present study may have a Ce concentration 1–2 orders of magnitude lower than anticipated [23]. This may explain the severe red shift in LuAG:Ce seen in this experiment, but further analysis is warranted.

Figure 14. Previous results for LuAG:Ce show peak photon emission at 545 nm with a Ce concentration of 0.03%. This is in stark contrast to the 630 nm red shift measured in the current study, from [21].

[5]Chief of Department for Crystal Growth Technology at the Institute for Scintillation Materials, NAS of Ukraine. His team was responsible for the fabrication of all scintillator crystals used in this study.

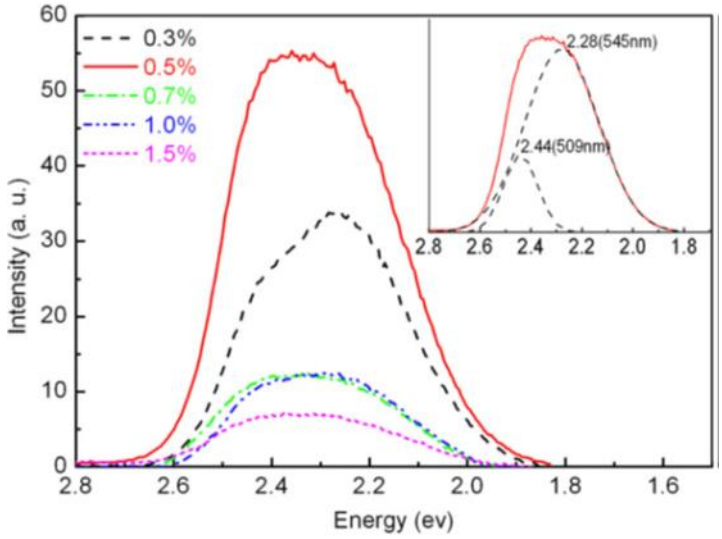

Figure 15. Red shift of spectral response for LuAG:Ce with decreased Ce concentration. Optimal concentration of 0.5% Ce is shown in red and 0.3% Ce is the black dotted line. Shift occurs from 509 nm to 545 nm, from [22].

Aside from the peak emission wavelength, the intensity of photon emission as a function of wavelength was calculated for the candidate set. As mentioned previously, the intensity of photon emission is a critical factor for scintillators. If photons emerge in the visible spectrum but are too weak or too broad, with no clearly identifiable peaks, efficiency and/or sensitivity will suffer. This can be due to the signal being lost in the background (too weak), or one that is generated across a wide wavelength band (too broad). Since the intensity of photon emission is proportional to the intensity of the incident energy, arbitrary units are generally assigned in the literature when presenting CL findings, as seen in Figures 15 and 16. However, since all of the crystals in this study were subjected to the same parameters, a comparison in photon intensity is certainly in order.[6]

With an incident electron energy of 5 keV, the photon intensity for the crystals ranged from approximately 30 photons/s at peak emission for ZWO to approximately 7500 photons/s for BGO. The tungstate based crystals as a group exhibited the lowest

[6] The only variable encountered for the candidate set of crystals is the physical dimensions of the samples. Width of the crystal will influence the response, but for the purposes of this study it assumed to be negligible.

intensity while BGO and the Ce activated crystals displayed the highest. Figure 16 shows the intensity recorded for ZWO and PWO. The erratic and noisy spectrum is attributed to low light yield according to [23]. Although PWO has a low light yield, it has the fastest response time (6 ns) of the candidate set [14, p. 66]; four orders of magnitude faster than ZWO; three orders faster than CWO; two orders faster than BGO; and one order faster than LuAG:Ce and LGSO:Ce [14].

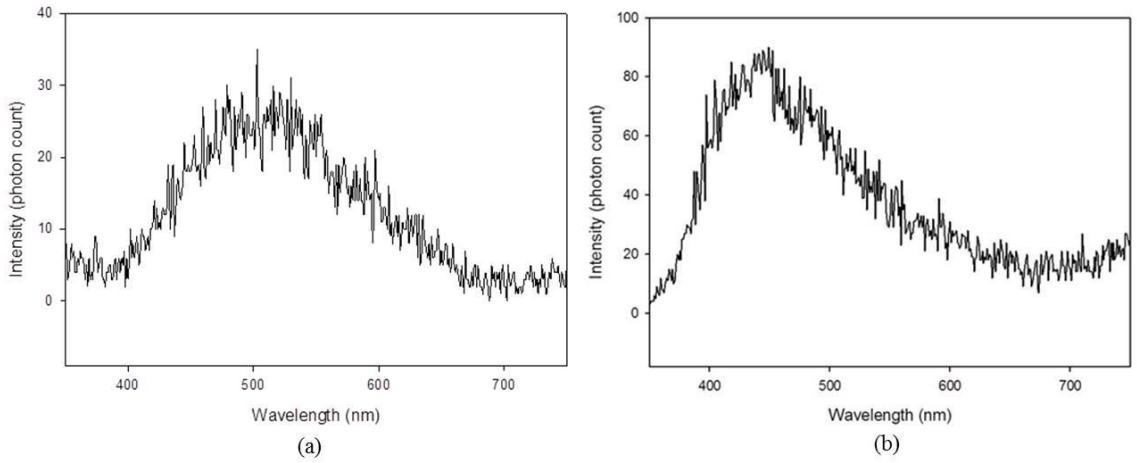

Figure 16. Intensity as a function of wavelength for ZWO (a) and PWO (b) at 5 keV electron beam incident energy. The noisy signal is attributed to low light yield in these scintillators.

The results for CWO and BGO, shown in Figure 17, indicate a stronger signal and good peak formation. The increased signal intensity for CWO compared to the other tungstate crystals is partially explained in [14, pp. 54–55] due to a high conversion factor of 0.01 electrons per incident eV. The conversion factor for BGO is even higher at 0.045 electrons per eV. With a greater number of free or quasi-free electrons in the crystal lattice, the greater the potential for photon emission. However, it is worth noting that no single factor fully explains photon emission. Several competing processes occur in the crystal during periods of stimulation that affect performance, and although the tungstate crystals share a similar chemical composition, their crystalline structures are different. In fact, CWO has a monoclinic structure P21/c, and is more similar structurally to LGSO [23].

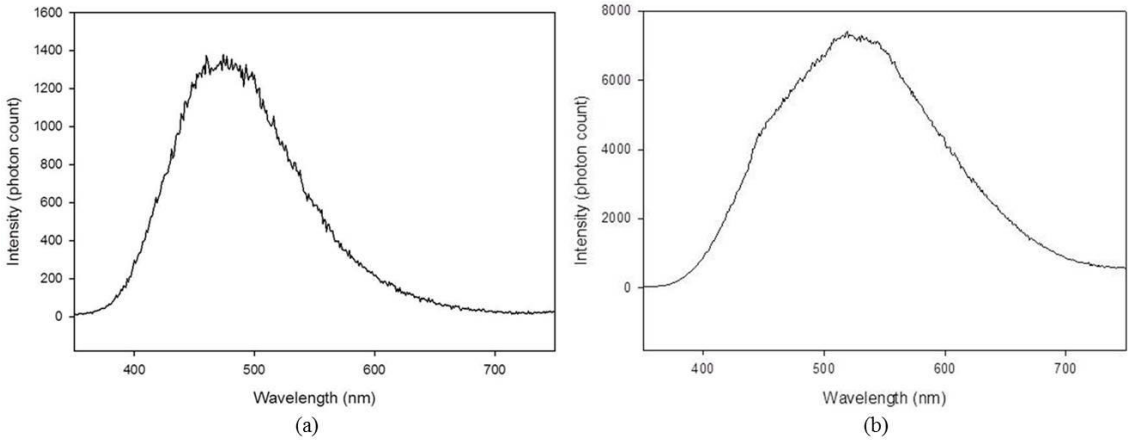

Figure 17. Intensity as a function of wavelength for CWO (a) and BGO (b) at 5 keV electron beam incident energy. Increased intensity is achieved in these crystals in part due to a high conversion factor of electrons per incident eV.

Based on the previous discussion concerning extrinsic luminescent scintillators (see Role of Activators in Chapter II), activated crystals generally exhibit a strong luminescent signal due to the formation of transition sites within the bandgap region of the scintillator (Figure 8). The concentration of the activator plays a tremendous role not only in the peak emission wavelength, but also in the intensity of the resulting photons [21]. This is clearly seen in Figure 16 for LuAG:Ce, where a 0.2% increase concentration of Ce, up to the optimal concentration of 0.5%, resulted in nearly a 55% increase in intensity [22]. The impact of Ce concentration does not, however, appear to affect the intensity of all activated crystals in the same manner, as Figure 18 shows for LGSO:Ce [24]. The spectral response for LGSO:Ce in this study, shown in Figure 19 (a), is in strong agreement with the literature and Figure 18 [24], at a Ce concentration of 0.3%.

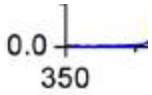

Figure 18. Previous study detailing the intensity as a function of wavelength for LGSO:Ce. The activator concentration does not affect the luminescent intensity as drastically as other activated scintillator crystals, from [24].

Figure 19 (b) for LuAG:Ce shows the uncontrolled admixture of Eu^{3+} ions in the crystal [23]. CL is well suited for identifying contaminants that can lead to false positive responses. When the bright emission at ~ 625 nm is disregarded, the maximum intensity of approximately 3600 photons/s is less than that of LGSO:Ce and according to [23], may be due to the low Ce concentration.

The CL measurements in this study confirmed the peak emission wavelengths for the candidate set of crystals, and identified the red shift in LuAG:Ce. All crystals displayed peak emission within the visible spectrum. When comparing the luminescent intensity, the tungstate crystals suffered from low light output, even with CWO's relatively high conversion factor. The activated crystals of LGSO and LuAG registered strong signals at around 4000 photons/s, but BGO performed best at nearly 7500 photons/s. The self-activating qualities of BGO and high conversion factor clearly contributed to the high rate of light output.

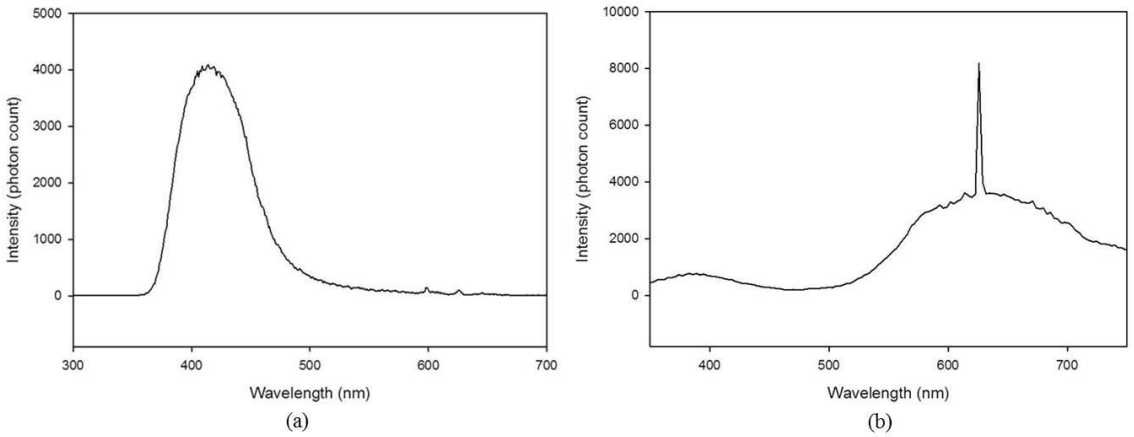

Figure 19. LGSO:Ce (a) displays a conventional spectral response and good luminescent intensity. Lower than optimal Ce concentration in LuAG:Ce (b) reduces luminescent intensity by about 10% when compared to LGSO:Ce.

C. GAMMA INDUCED SCINTILLATION

The culminating experiment in this study was designed to quantify the candidate crystals' scintillation response when subjected to radiation. Although a fast neutron source was preferred in order to confirm the inelastic scattering process, one was not currently available for use. Instead, gamma radiation sources were used to simulate the gamma photons normally resulting from the inelastic scattering event.[7]

1. Laboratory Setup

The apparatus used to quantify the gamma induced scintillation is shown in Figure 20, and was part of a dark room setup intended to minimize stray photon interference. The photomultiplier tube (PMT) is a thermoelectrically cooled Hamamatsu H7421-40 with a spectral response from 300–720 nm. It features a GaAsP photocathode with a quantum efficiency of 40% at peak wavelength of 580 nm. The Hamamatsu software was programmed to record photon counts in 100 ms intervals during the 180 s run time, for a total of 1800 data points.

[7] Testing with sources of fast neutrons is certainly necessary in future work. However, most spontaneous fission isotopes emit gamma radiation in addition to neutrons. This experiment has merit from the standpoint that incident gamma radiation is present from the onset of spontaneous fission, as well as from fast neutron inelastic scattering.

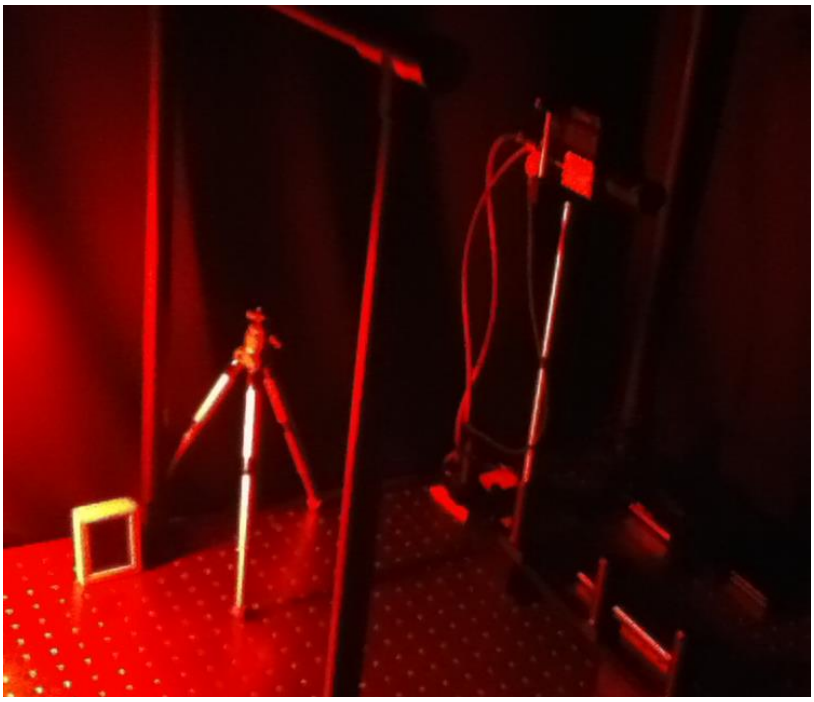

Figure 20. Hamamatsu H7421-40 PMT as part of a dark room laboratory setup used to measure the gamma scintillation response for the candidate set of crystals.

The source of radiation was provided using Co-60 and Ba-133 sources. Table 4 provides general information concerning these sources, to include current activity due to decay, and the average gamma energy based on the abundance of photons emitted. The deposited energy in Table 5 was determined to provide an approximation of the relative amount of energy delivered to each crystal based on isotope source, and should be considered preliminary in its reported values. Alternative calculations using air as the irradiated volume were considered, with the assumption that air would act as a surrogate for the relative energy deposition from the two sources. In both instances, Co-60 was found to deliver approximately 3.5 times more energy than Ba-133, yet stimulated less light output in the majority of the crystals. Only ZWO produced a higher scintillation when subjected to Co-60.

Table 4. General information for the radiation sources used in the gamma scintillation experiment, after [25].

	Co-60	Ba-133
Initial Activity (μCi)	1.0	1.0
Half-life (yrs.)	5.27	10.51
Date of Manufacture	Oct. 2006	Oct. 2007
Current Activity (μCi)	0.34	0.62
Gamma output MeV (% abundance)	1.173 (100); 1.333 (100)	0.081 (31); 0.303 (18); 0.356 (62)
Ave. Gamma Energy (MeV)	1.25	0.266
Ave. Gamma Energy per Disintegration (MeV)	2.50	0.300

Table 5. The estimated amount of deposited energy in the crystals.[8]

	Mass of Crystal (g)	Delivered Energy from Co-60 (MeV/s)	Delivered Energy from Ba-133 (MeV/s)
PWO	42.2	3.23e4	9.08e3
BGO	50.8	3.89e4	1.09e4
ZWO	63.4	4.85e4	1.36e4
CWO	64.3	4.92e4	1.38e4
LuAG:Ce	21.2	1.62e4	4.56e3
LGSO:Ce	22.6	1.73e4	4.86e3

2. Results

Based on Equation (8), [14] provides scintillation light yield values for common inorganic scintillators. These values were used to order the candidate set of crystals from lowest to highest expected light output: PWO, BGO, LuAG:Ce, CWO, ZWO, LGSO:Ce.[9] Table 6 provides these relative light output values, as well as the expected light yield from each radiation source based on delivered energy from Co-60 and Ba-133.

[8] Deposited energy was estimated by calculating the dose from the sources in units of Rads using the RadPro calculator (www.radprocalculator.com) and then converting this into absorbed energy in MeV for each of the crystals.

[9] Although the ordering of crystals was generally observed, the numerical values for light yield were not. For each of the crystals, a normalized light output was determined by multiplying the given crystal's relative light output value, given in [14], by the average gamma energy per disintegration from Table 4. Results are shown in Table 6. It is recognized that not all of the gamma energy from a single disintegration would be deposited in the crystal, but this calculation provides a basis for relative comparisons between the crystal responses.

Although the ordering was generally observed from the experimental data (with two exceptions discussed later), the expected light yield based on photon energy for the sources was not. As discussed later, a nonproportional response was observed that warrants additional research.

Table 6. Normalized light output values for crystals based on average gamma energy per disintegration for Co-60 and Ba-133, after [14].

	Relative Light Value (ph/MeV) [14], [26]	Expected Light Yield for Co-60 (photons)	Expected Light Yield for Ba-133 (photons)
PWO	100	250	30
BGO	8,200	20,500	2,460
ZWO	21,500	53,750	6,450
CWO	19,700	49,250	5,910
LuAG:Ce	14,000	35,000	4,200
LGSO:Ce	21,300	53,250	6,390

Figure 21 provides the experimental results for the intrinsic (non-activated) scintillator crystals. According to [14], PWO has a very weak light yield, as recorded in Table 6. Referring to Figure 21 (a), PWO exhibited the lowest photon count in the experiment with both gamma sources generally producing about the same light output despite the fact that the rate of delivered energy from the two sources differed significantly. The relative light yield for BGO is likewise considered marginal [14], but a clear stratification in photon count between Co-60 and Ba-133 was observed. Referring to Table 6 and Figure 21 (d), the expected light output for Co-60 and Ba-133 was not attained. In fact, Ba-133 actually produced a higher light output than Co-60. This trend was consistently seen in all of the crystals with the exception of ZWO.

According to [14], ZWO has the highest light yield of the tungstate group; however, the experimental results are not consistent and show a lower light yield than CWO. ZWO did display the unique property of greater light output from Co-60 than from Ba-133, and is the only crystal to exhibit this phenomenon. This may be due in part to the difference in physical size of the crystal sample. ZWO and CWO are the only crystal samples with cubic dimensions, as shown in Table 1. Sample dimensions are discussed in

greater detail beginning on page 35. CWO achieved the second highest light output of the tested crystals, and stratification was not as prevalent as in the other intrinsic luminescent scintillators. Figure 21 (c) indicates that CWO was more likely to produce a constant light output as a function of incident photon energy, but again significantly less than the expected light output values from Table 6. As explained in the CL results, CWO has a crystalline structure similar to LGSO:Ce, which may explain their similarities in both the CL and gamma induced scintillation results.

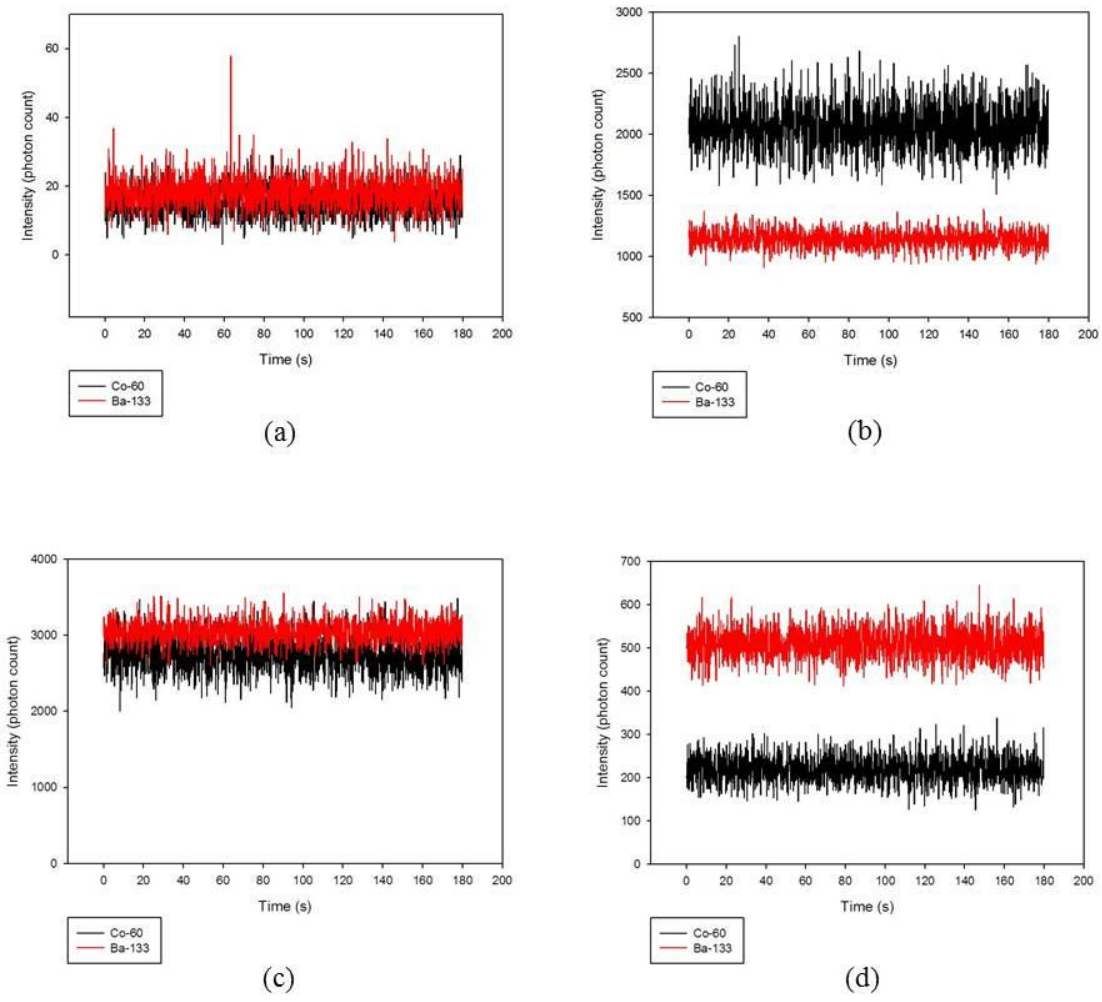

Figure 21. Photons emitted from gamma induced scintillation in 100 ms intervals for PWO (a), ZWO (b), CWO (c), and BGO (d). Stratification based on incident gamma photon energy is most pronounced in ZWO and BGO.

Based on the discussion from Chapters I and II, the activated crystals should produce a high light output. Due mainly to the presence of activator sites within the bandgap region of the crystalline structure, activated crystals are specifically designed to increase light yield [13]. Figure 22 presents the experimental results for LuAG:Ce and LGSO:Ce. The experimental data for LuAG:Ce indicates extremely poor light output. Referring to the results from the CL measurement, the apparent lack of correct Ce concentration most likely explains the low light yield.[10] A stratification in light output is seen, but further testing with additional LuAG:Ce crystal samples of definitive Ce concentration is necessary before analysis can made.

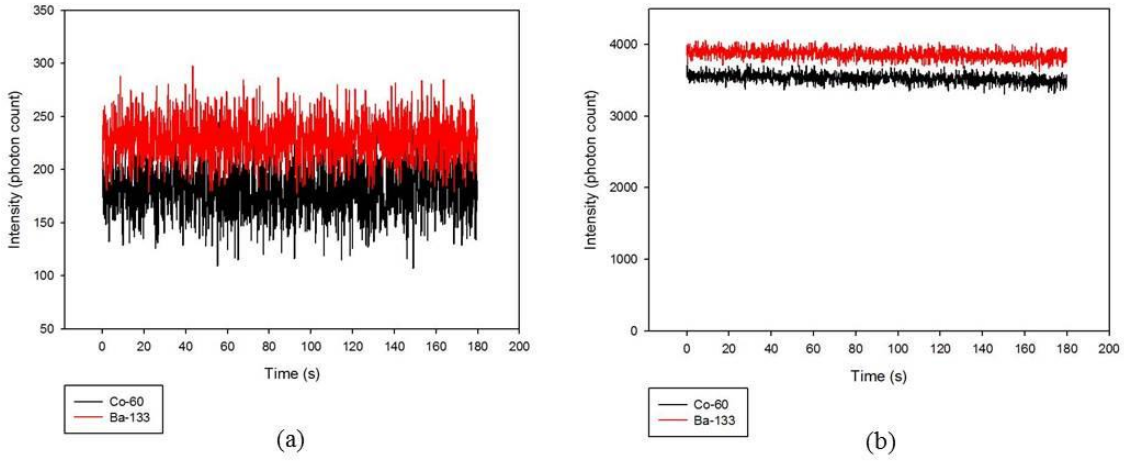

Figure 22. Photons emitted from gamma induced scintillation in 100 ms intervals for LuAG:Ce (a) and LGSO:Ce (b). LuAG:Ce exhibited poor scintillation due to a low Ce concentration while LGSO:Ce displayed the highest light yield of the candidate set.

Although LGSO:Ce attained the highest light output in the study, the results are not consistent with neither the relative light output value nor the expected light yield values given in Table 6. Similar to CWO, the light output in LGSO:Ce appeared to be fairly constant. Although a slight stratification exists, LGSO:Ce appeared better suited to scintillate at both tested gamma energies. To further investigate this point, LGSO:Ce was

[10] According to Dr. Oleg Sidletskiy, the LuAG:Ce sample used in this study had a 1–2 order of magnitude lower than anticipated Ce concentration.

subjected to an additional gamma source, Na-22 with a single 1.275 MeV gamma photon. The results shown in Figure 23 display the slight stratification between each gamma source, and a trend that suggests a non-intuitive inverse relationship between incident gamma energy and light output. Although further testing is required to confirm this observation, it appears that LGSO:Ce is efficient in scintillation at varying gamma energies. A possible explanation lies in the increased scattering mean free path for higher energy gammas combined with the relatively small dimensions of the crystals.

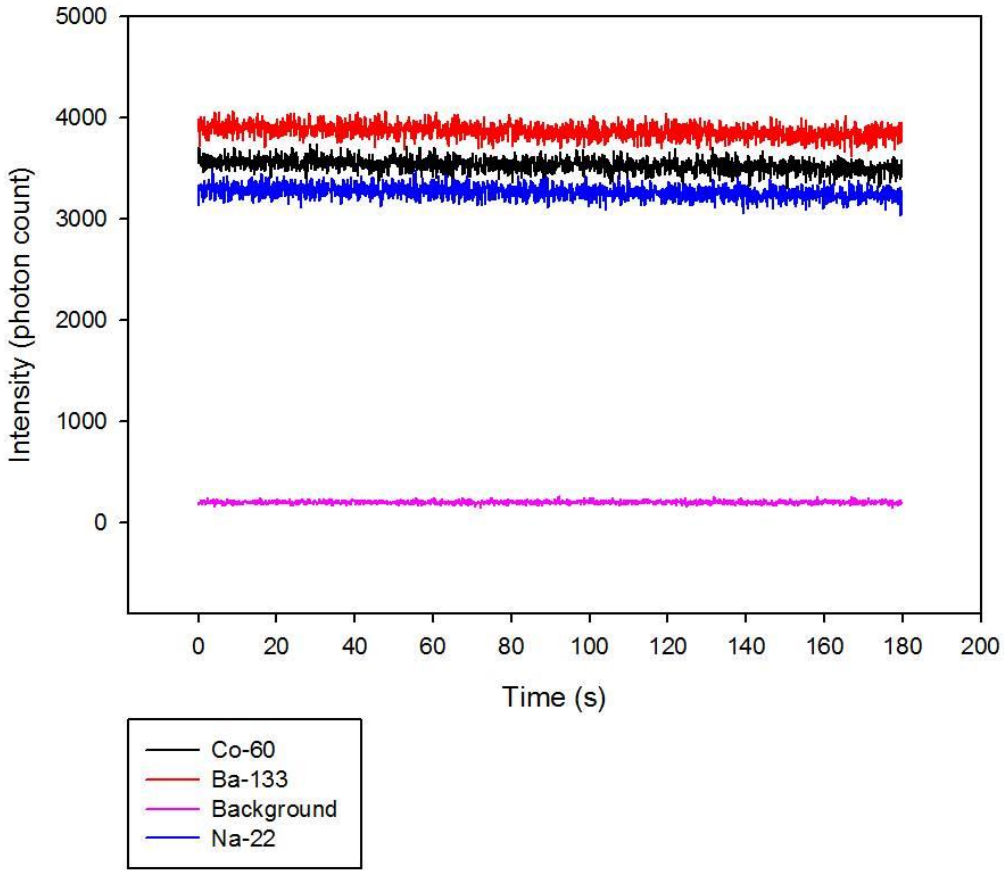

Figure 23. Photons emitted from LGSO:Ce in 100 ms intervals using three different gamma radiation sources. Although efficient in light output at varying incident energies, an inverse dependency may exist for LGSO:Ce and other crystals.

The experimental results from the gamma induced scintillation provide an abundant source of information on the performance of the crystals. One noteworthy observation involves the relatively small size of the crystals and their ability to absorb the incident gamma energy. CWO and ZWO produced the highest light output of the non-activated scintillator crystals in this experiment. They also have cubic dimensions that make their volume much larger than any other crystal studied. With a thickness twice that of the other crystals, it is reasonable to predict that incident gamma photons were absorbed at a higher rate, thereby facilitating a higher light output. Larger crystal dimensions will lead to a greater amount of deposited energy, since higher energy gamma photons have more penetrating power and greater mean free paths. However, the activated crystal LGSO:Ce achieved light output similar to that of the best performing non-activated crystal (CWO), at half the thickness. This observation supports the notion that activated crystals produce higher light output than non-activated, but further testing with uniform samples or computer modeling that incorporates crystal dimensions is necessary to support this claim.

The experimental results also bring into question the relationship involving incident photon energy, the amount of energy deposited within the crystal and the expected light output. As mentioned previously, the energy deposited in the crystal is generally released via visible light emission in scintillators, but that trend was not generally witnessed during the conduct of this experiment. The relative light yield provided in [14], when normalized to the average gamma energy per disintegration for Ba-133 and Co-60, was only slightly observed in some cases involving Ba-133, and is most likely a result of coincidence. The expected light output for each crystal when subjected to Co-60 was significantly lower in each instance, and is likely due to the nonproportional response described by Rodnyi [13, pp. 46–49]. The nonproportional response is an intrinsic property of scintillators, and is not fully understood [13]. The conventional belief that higher incident photon energy will result in a proportional response does not apply at all energy ranges and in all types of crystals [13]. Further testing with a wider range of incident gamma energies will aid in the understanding of scintillator response.

THIS PAGE INTENTIONALLY LEFT BLANK

IV. CONCLUSIONS

A. SUMMARY

Neutron detection technology was historically advanced based on the needs to support scientific inquiry and the nuclear power establishment. Detectors designed to identify thermal and slow neutrons based on absorption or elastic scattering reactions were modified to allow for the detection of fast neutrons, albeit inefficiently. With the current global concern surrounding nuclear proliferation and the ever increasing threat posed by improvised nuclear devices, it is essential that fast neutron detection be improved for efficient use in security and nonproliferation applications.

One possible solution involves the use of heavy oxide inorganic scintillators to efficiently detect fast neutrons. These scintillators provide both the inelastic scattering event, resulting in the emission of gamma photons, and their subsequent scintillation response that can be coupled to an electronic detector unit. Preliminary studies indicate that efficiency can reach 70–80% for gamma radiation and not less than 40% for fast neutrons, a vast improvement from the current 10% efficient models of today [3].

In this thesis, the theory of neutron interactions was discussed with special emphasis on inelastic scattering. Scintillation and the role of activators were also examined as they pertained to the candidate set of crystals. The experimental portion of this thesis was intended to provide a more thorough understanding of the optical, cathodoluminescence and gamma induced scintillation properties of PWO, ZWO, CWO, BGO, LuAG:Ce and LGSO:Ce. The optical measurements verified that a high rate of transmittance occurred in each crystal, with minimal absorption or internal reflection. All crystals performed well with transmittance averaging about 80% with less than 3% absorption. The results from the CL measurements confirmed the peak wavelengths for each crystal based on the literature, and identified a severe red shift in the LuAG:Ce sample, attributed to a low Ce concentration. The gamma induced scintillation experiment provided preliminary results for the scintillation response of each crystal based on incident gamma energies in the range of 0.081–1.275 MeV. Experimental

results raise the question of nonproportionality qualities inherent to the scintillator crystals.

B. FUTURE RESEARCH

The preliminary results from the characterization of the six candidate crystals in this study is the first step in achieving a better understanding of how heavy oxide inorganic scintillators can be used in the detection of fast neutrons. The ideal scintillator does not currently exist, so considerations such as light yield, response time, temperature dependence, detection range and size must be evaluated in order to fully understand the mechanics of scintillation in the context of fast neutron detection. Preliminary findings in this study indicate a strong correlation between crystalline structure and light yield. The similarities in response to CL and gamma induced scintillation for CWO and LGSO:Ce, crystals with vastly different chemical composition but similar structure, is a topic worthy of future work.

Although much effort was made to calculate the amount of energy deposited in the crystals during the gamma induced scintillation experiment, only preliminary estimates were achieved. The ability to ascertain the deposited photon energy, based on source activity and average gamma energy per disintegration, will allow for the direct comparison with cited sources from the literature.

Testing with a source of fast neutrons is necessary in order to examine the inelastic scattering event and subsequent scintillation within the crystals. Although the crystals in this study were shown to respond well to various other forms of radiation, fast neutrons are the crux of the overall study, and every effort should be made to test with them.

LIST OF REFERENCES

[1] Office of the White House. (2010, May 26). *National Security Strategy.* [Online]. Available: http://www.whitehouse.gov/sites/default/files/rss_viewer/national_security_strategy.pdf

[2] D. Philips, "Transport imaging of spatial distribution of mobility-lifetime product in bulk semiconductors for nuclear radiation detection," Ph.D. dissertation, Dept. of Phys., Naval Postgraduate School, Monterey, CA, 2012.

[3] V. D. Ryzhikov et al., "High efficiency fast neutron detectors based on inorganic scintillators," presented at IEEE Nuclear Science Symp., Seattle, WA, 2014.

[4] V. D. Ryzhikov et al., "The neutron detectors based on oxide scintillators for control of fissionable radioactive substances," *Proc. of SPIE,* vol. 9213, pp. 92131B-1-92131B-7, 2014.

[5] G. Knoll, *Radiation Detection and Measurement,* 3rd ed. Hoboken, NJ: John Wiley & Sons, 2000.

[6] K. Krane, *Introductory Nuclear Physics.* Hoboken, NJ: John Wiley & Sons, 1988, pp. 444–476.

[7] N. Ensslin, "The origin of neutron radiation," in *Passive Nondestructive Assay of Nuclear Materials*, T. D. Reilly et al., Ed., Los Alamos, NM: U.S. Nuclear Regulatory Commission NUREG/CR-5500 (also LA-UR-90-732), 1991, pp. 337–354.

[8] A. B. Smith and P. R. Fields, "Spontaneous fission neutron spectrum of Cf^{252}," *Physical Review*, vol. 108, no. 2, pp. 411–413, Oct. 1957.

[9] K. W. Beckurts and K. Wirtz, *Neutron Physics.* Berlin, Germany: Springer, 1964, ch. 13, pp. 286–295.

[10] T. W. Crane and M. P. Baker, "Neutron Detectors," in *Passive Nondestructive Assay of Nuclear Materials*, T. D. Reilly et al., Ed., Los Alamos, NM: U.S. Nuclear Regulatory Commission NUREG/CR-5550 (also LA-UR-90-732), 1991, pp. 379–406.

[11] Interaction of Neutrons with Matter. (n.d.). U.S. Nuclear Regulatory Commission and Duke University. [Online]. Available: https://www.safety.duke.edu/RadSafety/drdl/modules/rp/10_rp.pdf. Accessed Jan. 19, 2015.

[12] V. D. Ryzhikov et al., "New neutron detectors based on inorganic scintillators using inelastic scattering," in *IEEE Nuclear Science Symp*, Orlando, FL, 2009, pp. 1978–1982.

[13] P. Rodnyi, *Physical Processes in Inorganic Scintillators.* Boca Raton, FL: CRC Press, 1997, ch. 1, pp. 1–51.

[14] P. Lecoq et al., *Inorganic Scintillators for Detector Systems.* Berlin, Germany: Springer, 2006.

[15] Luminescence generation and nomenclature. (n.d.). Commonwealth Scientific and Industrial Research Organization. [Online]. Available: http://www.csiro.au/luminescence/about.html. Accessed Jan. 19, 2015.

[16] G. Karunasiri, private communication, Jan. 2015.

[17] SpectraSuite spectrometer operating software installation and operation manual. (n.d.). Ocean Optics, Inc. [Online]. Available: http://oceanoptics.com/wp-content/uploads/SpectraSuite.pdf. Accessed Feb. 6, 2015.

[18] F. L. Pedrotti and L. S. Pedrotti, *Introduction to Optics*, 2nd ed. Upper Saddle River, NJ: Prentice Hall, 1993, ch. 20, sec. 20–4, pp. 417–419.

[19] R. Mao et al., "Optical and scintillation properties of inorganic scintillators in high energy physics," *IEEE Transactions on Nuclear Science*, vol. 55, no. 4, Aug. 2008.

[20] Cathodoluminescence theory. (n.d.). Montana State University Science Education Resource Center at Carleton College. [Online]. Available: http://www.serc.carleton.edu/research_education/geochemsheets/CLTheory.html. Accessed Feb. 5, 2015.

[21] A. Setlur et al., "Blue light-emitting diode phosphors based upon oxide, oxyhalide and halide hosts," *ECS J. Solid State Sci. Tech.*, vol. 2, no. 2, pp. R3059–R3070, 2013.

[22] H.-L. Li et al., "Luminescent properties of LuAG:Ce phosphors with different Ce contents prepared by a sol-gel combustion method," *Optical Materials*, vol. 29, no. 9, pp. 1138–1142, May 2007.

[23] O. Sidletskiy, private communication, April 2014.

[24] O. Sidletskiy et al., "Impact of Lu/Gd ratio and activator concentration on structure and scintillation properties of LGSO:Ce crystals," *J. Crystal Growth*, vol. 312, no. 4, pp. 601–606, Feb. 2010.

[25] Radionuclide data sheets. (n.d.). University of California, San Diego. [Online]. Available: https://ehs.ucsd.edu/rad/radionuclide/radionuclide_datasheets.html. Accessed Mar. 4, 2015.

[26] B. Grinyov et al., “Absolute light yield determination for LGSO:Ce, CWO, ZnSe:Al, and GSO:Ce crystals,” *IEEE Transactions on Nuclear Science*, vol. 57, no. 3, June 2010.

THIS PAGE INTENTIONALLY LEFT BLANK

INITIAL DISTRIBUTION LIST

1. Defense Technical Information Center
   Ft. Belvoir, Virginia

2. Dudley Knox Library
   Naval Postgraduate School
   Monterey, California